

# CaLiV: LiDAR-to-Vehicle Calibration of Arbitrary Sensor Setups via Object Reconstruction

Ikir Tahiraj<sup>1,\*</sup>, Markus Edinger<sup>2</sup>, Dominik Kulmer<sup>1</sup>, Markus Lienkamp<sup>1</sup>

**Abstract**—In autonomous systems, sensor calibration is essential for a safe and efficient navigation in dynamic environments. Accurate calibration is a prerequisite for reliable perception and planning tasks such as object detection and obstacle avoidance. Many existing LiDAR calibration methods require overlapping fields of view, while others use external sensing devices or postulate a feature-rich environment. In addition, Sensor-to-Vehicle calibration is not supported by the vast majority of calibration algorithms. In this work, we propose a novel target-based technique for extrinsic Sensor-to-Sensor and Sensor-to-Vehicle calibration of multi-LiDAR systems called CaLiV. This algorithm works for non-overlapping FoVs, as well as arbitrary calibration targets, and does not require any external sensing devices. First, we apply motion to produce FoV overlaps and utilize a simple unscented Kalman filter to obtain vehicle poses. Then, we use the Gaussian mixture model-based registration framework GMMCalib to align the point clouds in a common calibration frame. Finally, we reduce the task of recovering the sensor extrinsics to a minimization problem. We show that both translational and rotational Sensor-to-Sensor errors can be solved accurately by our method. In addition, all Sensor-to-Vehicle rotation angles can also be calibrated with high accuracy. We validate the simulation results in real-world experiments. The code is open source and available on <https://github.com/TUMFTM/CaLiV>.

## I. INTRODUCTION

Fusion of sensor data is essential for autonomous robots to interpret their environment. Multi-sensor fusion relies on extrinsic sensor calibration to accurately align sensor measurements. Inaccurate sensor calibration can propagate through the autonomous system, affecting not only fusion tasks such as object detection, but also safety-critical downstream processes such as planning and control [1].

The performance of sensor fusion tasks relies primarily on accurate Sensor-to-Sensor (S2S) calibration. However, the global position accuracy of the fused data is highly dependent on Sensor-to-Vehicle (S2V) calibration, making S2V calibration particularly important for downstream tasks such as planning, where accurate object and obstacle positions are required. S2V involves estimating calibration parameters relative to a vehicle or base frame, rather than between individual sensors. In the current state of the art, sensor calibration is primarily addressed in the S2S context. S2V calibration approaches have not received much attention from the research community, even though it has a major impact on the overall system performance and safety.

\* Corresponding author [ilir.tahiraj@tum.de](mailto:ilir.tahiraj@tum.de)

<sup>1</sup>Authors are with the TUM School of Engineering and Design, Chair of Automotive Technology, Technical University of Munich.

<sup>2</sup>with the TUM School of Computation, Information and Technology, Technical University of Munich.

Unlike conventional S2S approaches, there are no directly comparable measurements available to find correspondences between a sensor frame and a vehicle frame to perform a calibration. Therefore, almost all S2V calibration frameworks use motion-based approaches such as Simultaneous Localization and Mapping (SLAM) or hand-eye calibration to solve the S2V problem. This is primarily because the motion itself serves as the correspondence to be identified between the sensor and the vehicle.

A similar problem occurs in sensor calibration when dealing with non-overlapping sensor setups. The calibration becomes significantly more challenging with sensors that do not share a common field of view and, therefore, never simultaneously observe the same features. This is common in applications involving large vehicles, such as buses or trains. Accordingly, non-overlapping sensor calibration frameworks also use motion-based methods, including SLAM or hand-eye calibration.

SLAM-based calibration methods generate a map of the environment through point cloud matching and implicitly solve for the extrinsic parameters. These approaches rely heavily on environmental features, which may not always be available. Hand-eye calibration [2] methods are less dependent on specific environmental features, but do not achieve the calibration accuracy of SLAM algorithms [3]. In addition, these motion-based methods are commonly presented as targetless calibration techniques [4], [5]. Although these targetless approaches offer greater flexibility, they still do not match the accuracy of target-based solutions [6]. In contrast, target-based S2V or non-overlapping S2S calibration has mainly been addressed using external sensing devices [7], [8], [9].

In this work, we present CaLiV, a two-stage calibration method as a target-based approach to address the problems of S2V calibration for an arbitrary sensor setup without any additional external sensing devices. The first stage aims to perform (non-overlapping) S2S calibration. The second stage utilizes the S2S calibration to compute the S2V calibration parameters. As the underlying alignment model, we rely on GMMCalib [10], which provides a specific reference frame formulation for simultaneous optimization of the S2V calibration parameters. The approach is illustrated in Fig. 1. Our contributions are as follows:

- To the best of our knowledge, we are the first to present an open-source target-based Sensor-to-Vehicle calibration framework for a multi-LiDAR sensor setup without any external sensor devices.
- In addition, our approach is the first to simultaneously

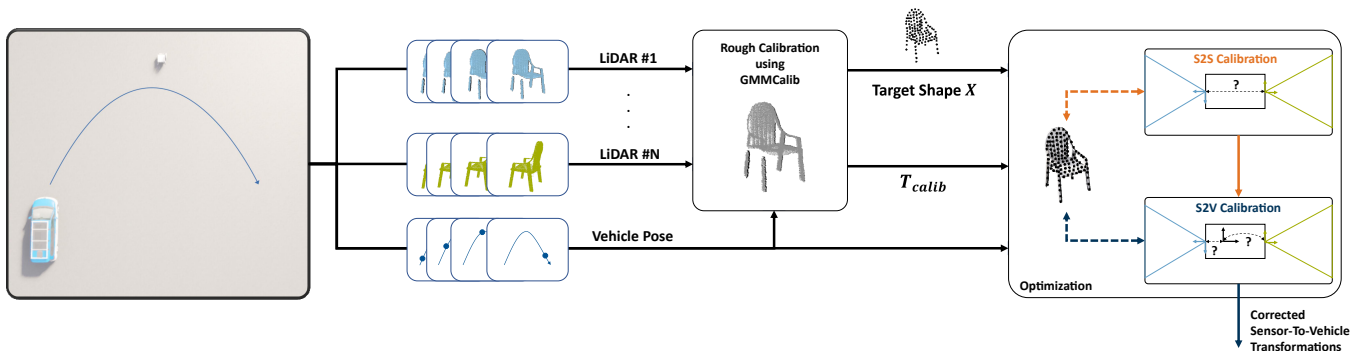


Fig. 1: CaLiV: Data is collected by driving a curved trajectory. The data is first aligned using vehicle poses and different perspectives of the calibration target. In the optimization phase, the algorithm first computes the S2S calibration, which serves as input for the S2V optimization. The input to the S2S and S2V optimization is a calibration matrix and the shape of the reconstructed target, both generated using GMMCalib [10], as well as the vehicle poses from an unscented Kalman Filter (UKF).

allow for Sensor-to-Sensor calibration of arbitrary sensor setups.

- We utilize a joint registration method and incorporate target reconstruction to perform Sensor-to-Vehicle calibration using a reference frame formulation as presented in GMMCalib.
- We evaluate the Sensor-to-Sensor and Sensor-to-Vehicle performance of our method on a worst-case sensor setup with two LiDAR sensors facing in opposite directions in simulation and real-world experiments. We outperform the current state-of-the-art for both non-overlapping Sensor-to-Sensor and Sensor-to-Vehicle calibration.

## II. RELATED WORK

There have been many advances in extrinsic calibration in recent years, addressing S2S and S2V calibration with different sensor setups and overlapping FoVs. To present the current state of the art, the contributions on extrinsic sensor calibration will be categorized in targetless and target-based approaches.

### A. Targetless Calibration

In many cases, targetless approaches perform feature-based calibration using geometric features of the environment. For example, the works of [11], [12], [13], and [14] present S2S calibration using different features such as edges, planes or corners. In the same context, feature-based approaches as presented in [15], [16], [17], and [18] are often used to perform S2V calibration. In [15], road edges are used to compute the roll and pitch angle errors of the sensor relative to the robot frame. Kulmer *et al.* [16] and Yan *et al.* [18] use the ground plane to perform a partial S2V calibration that compensates for the roll and pitch angle errors. In addition, the z-coordinates are computed in [16] and [18] respectively.

Targetless calibration can also be performed using motion-based or mapping-based methods. The general idea of motion-based calibration is that the motion of a robot can be used to identify the extrinsics of the sensors by exploiting the rigid body assumption. This is typically done by solving a

matrix equation of the form  $AX = XB$ , where  $X$  is unknown. Solving this problem is also referred to as the hand-eye calibration problem [2]. Das *et al.* [3] use the hand-eye formulation to calibrate multiple non-overlapping LiDARs. Similarly, in [19], [20], and [21], this formulation is used to recover the sensor extrinsics. In [5], a S2V framework is introduced using the hand-eye formulation to describe the relationship between the vehicle frame and the LiDAR frame.

In contrast to motion-based calibration methods, mapping-based methods use features of the environment directly for the calibration task. This can be done, for example, by simultaneously creating a map of the environment, estimating the robot’s pose relative to this map, and recovering the extrinsic parameters of the sensors in a SLAM-based application as presented in [4] and [22]. The mlcc framework presented in [23] simultaneously optimizes the LiDAR poses and sensor parameters by matching point clouds with an adaptive voxelization technique.

As mentioned in the introduction, relying on S2S calibration only is not sufficient for safe autonomous operation. In the current landscape, some of the approaches only partially fulfill these requirements by providing either S2S calibration for non-overlapping FoVs or S2V calibration. While [5] supports S2V calibration for large vehicles using hand-eye calibration and thus implicitly calibrates non-overlapping sensor setups, the calibration does not achieve state-of-the-art translation and rotation accuracy. Although both motion-based and mapping-based calibration are well suited for non-overlapping S2S calibration, they currently do not provide accurate S2V calibration and require long motion sequences to recover the calibration parameters. S2V calibration is primarily solved by feature-based methods, which, due to the nature of the algorithms, require a feature-rich environment.

### B. Target-Based Calibration

Target-based calibration methods set up specific targets which are then scanned by all sensors. The resulting point clouds can then be matched using point cloud registration algorithms. To perform a target-based calibration, all sensors must see the target. For this reason, target-based

algorithms have mostly been used to calibrate sensors with overlapping FoVs, as for example in [24], [25]. In contrast, GMMCalib [10] shows potential for the calibration of non-overlapping FoVs due to its robustness to different perspectives. The first target-based calibration method to perform both S2S and S2V calibration was introduced by Domhof *et al.* [7]. They use a Styrofoam target with circular holes for S2S calibration and an additional external laser scanner for S2V calibration. By estimating the robot's body reference frame with this external sensor, they are able to perform S2V calibration without introducing motion. To perform a target-based calibration, all sensors must be able to see the target simultaneously or motion must be introduced to create an overlapping FoV. The first option, implemented by [9], uses a full environment scan as a reference map, created with an external terrestrial laser scanner. By aligning individual LiDAR point clouds to this map, S2S calibration errors are resolved without moving the system. However, S2V calibration remains unaddressed since some errors require motion to be observed [5].

The second option is a more suitable method to also solve S2V errors. Charron *et al.* [8] used this approach to calibrate a camera-LiDAR system. Both the target and system poses are recovered using an additional motion capture system (MCS). The dimensions of the target are measured beforehand so that specific key points can be identified. The ground truth positions of these key points are known by combining the target pose returned by the MCS with the dimensions of the target. This method could theoretically solve S2V calibration errors, depending on the system's trajectory relative to the target. Similar to [7] and [9], the work of [8] also presents highly accurate results with the help of an additional external sensor.

The state-of-the-art shows that for the above requirements, target-based approaches outperform targetless approaches in terms of calibration accuracy. However, this is mainly due to the use of external sensing devices and very specific calibration targets, which in some cases, as shown in [8], are even measured in advance. Accuracy is therefore achieved at the expense of the flexibility that can be provided by targetless approaches. We conclude that there is no target-based, environment-independent calibration framework for extrinsic S2V calibration of multi-LiDAR systems with non-overlapping FoVs. Therefore, to combine the advantages of both strategies, we propose a target-based calibration framework that makes use of feature-based and motion-based principles for S2V calibration as well as the ability to calibrate non-overlapping sensors. We achieve this with arbitrary targets and without the use of additional external sensor systems.

### III. METHODOLOGY

This section describes the methodology behind the framework of Fig. 1. For the sake of clarity, we consider the calibration with a vehicle with two non-overlapping LiDARs. However, the proposed technique can easily be generalized for any multi-LiDAR setup. In the following, the notation

of [26] is used to express all mathematical formulations related to homogeneous transformations.

#### A. Problem Statement

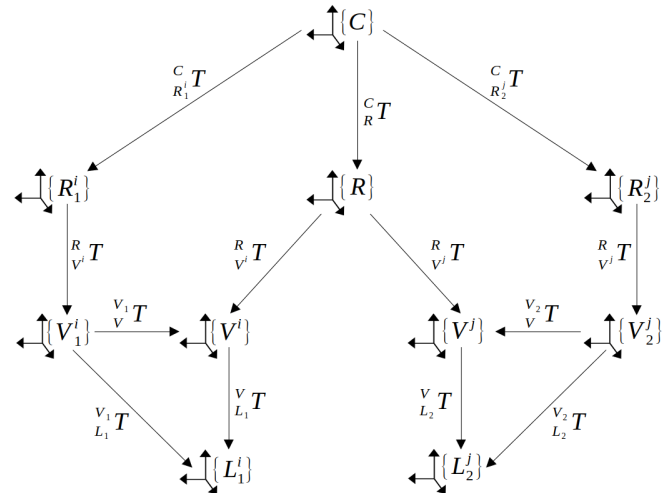


Fig. 2: Spatial relationship between the frames  $\{V^i\}$  and  $\{V^j\}$  of a moving system at a specific time steps  $t_i$  and  $t_j$  with two LiDAR frames  $\{L_1^i\}$  and  $\{L_2^j\}$ , a global reference frame  $\{R\}$ , and a common calibration frame  $\{C\}$ .

Fig. 2 shows the spatial relationships, relevant for the calibration task, for a moving vehicle  $V$  with two non-overlapping LiDARs  $L_1$  and  $L_2$ . In addition, we introduce the time step  $t_i$  for a measurement of  $L_1$  and the time step  $t_j$  for a measurement of  $L_2$  with  $1 \leq i, j \leq N$ .  $\{L_1^i\}$ ,  $\{L_2^j\}$ ,  $\{V^i\}$ , and  $\{V^j\}$  describe the respective LiDAR and vehicle frames at the time steps  $t_i$  and  $t_j$ .  $\{R\}$  represents the global reference frame and  $\{C\}$  the common calibration frame as introduced in [10].

${}^V_{L_1}T$  and  ${}^V_{L_2}T$  describe the ground truth transformations of the LiDARs relative to  $\{V\}$ . Correspondingly,  ${}^{V_1}_{L_1}T$  and  ${}^{V_2}_{L_2}T$  are the initial transformations that result in the erroneous vehicle frames  $\{V_1^i\}$  and  $\{V_2^j\}$  when applied to the sensors' point clouds. The S2V calibration errors of  $L_1$  and  $L_2$  are described by  ${}^{V_1}_{V^i}T$  and  ${}^{V_2}_{V^j}T$  respectively.

${}^R_{V^i}T$  and  ${}^R_{V^j}T$  represent the vehicle poses at time steps  $t_i$  and  $t_j$ . Applying these transformations to the erroneous vehicle frames  $\{V_1^i\}$  and  $\{V_2^j\}$  results in the erroneous versions  $\{R_1^i\}$  and  $\{R_2^j\}$  of the reference frame, that describe the propagation of a S2V error through the vehicle's motion. A registration algorithm is executed on point clouds in the frames  $\{R_1^i\}$  and  $\{R_2^j\}$ , which returns the calibration transformations  ${}^C_{R_1^i}T$  and  ${}^C_{R_2^j}T$  relative to the calibration frame.  ${}^C_R T$  represents the calibration frame error relative to the reference frame  $\{R\}$ . In this specialized dual-LiDAR version of the calibration problem,  ${}^C_R T$  can be computed as follows:

$${}^C_R T = {}^C_{R_a^i} T {}^R_{V^i} T {}^{V_a}_{V^i} T {}^{R_1^i}_{V^i} T^{-1} \quad (1)$$

$\forall i, a \quad s.t. \quad 1 \leq i \leq N, \quad a \in \{1, 2\}.$

Further, we define  $L_2$  to be the reference LiDAR and  ${}^{V_2}_{V^j}T$  to be the joint S2V error. The S2S calibration error of  $L_1$

relative to  $L_2$  is referred to as  $V_2^a T$ . The  $L_1$  S2V error is therefore defined as follows:

$$V_1 T = V_2 T^{-1} V_2^a T. \quad (2)$$

Since the S2V errors  $V_2^a T$  are not known, the ground truth value of  $C_R T$  cannot be computed directly. Therefore, we introduce  $C_R \bar{T}_a^i$  which describes the approximation of  $C_R T$  for the LiDAR  $L_a$  at time step  $t_i$  and an estimated S2V error  $V_2^a \bar{T}$ . In a non-overlapping setup, the respective LiDARs may not see the target at all time steps. Therefore, we define a set  $S$  as the set of all pairs of sensors and time steps for which such a transformation is given, i. e. the sensor sees the target. Specifically, we say  $(i, a) \in S$  iff  $C_{R_a} \bar{T}_a^i$  is known. The problem of recovering the extrinsic sensor parameters can now be reduced to the following minimization problem:

$$\left( V_2^a T, V_1 T \right) \approx \underset{\left( V_2^a \bar{T}, V_1 \bar{T} \right)}{\operatorname{argmin}} \sum_{\{(i,a), (j,b)\} \subset S} e(C_{R_a} \bar{T}_a^i, C_{R_b} \bar{T}_b^j), \quad (3)$$

where  $e$  is a function returning the error between a pair of transformations.  $V_2^a \bar{T}$  and  $V_1 \bar{T}$  correspond to the S2S and S2V errors and are optimized by the minimization algorithm. The optimal transformations  $V_2^a T$  and  $V_1 T$  are finally used to recover the sensor extrinsics  $V_{L_1} T$  and  $V_{L_2} T$ :

$$V_{L_1} T = V_1 T^{-1} V_1 T = V_2 T^{-1} V_2^a T V_{L_1} T \quad (4)$$

$$V_{L_2} T = V_2 T^{-1} V_2 T, \quad (5)$$

with  $V_{L_1} T$  and  $V_{L_2} T$  being the initial transformations of both LiDAR sensors given as an input to the algorithm.

### B. Implementation Details

We now present the implementation details of our framework used to solve the minimization problem formulated in Section III-A. Specifically, we discuss the kinematic model used to recover the vehicle poses  $R_{V_i} T$ , the joint registration algorithm used to obtain the transformations  $C_{R_a} \bar{T}_a^i$  of all point clouds to a common calibration frame  $\{C\}$ , as well as the minimization algorithm.

1) *Kinematic Model*: The approach is compatible with any kinematic model, provided that the vehicle poses are given at the time steps of the LiDAR measurements. Two sources of vehicle poses were used to validate the performance of the algorithm: The ground truth vehicle poses obtained from simulation and an unscented Kalman filter (UKF) [27]. The latter kinematic model is used to combine IMU, GPS, velocity and orientation data to recover vehicle pose estimates  $R_{V_i} T$  at all time steps  $t_i$ . The UKF also allows the modeling of sensor-specific noise and uncertainties to evaluate the calibration accuracy under noisy sensor data.

2) *Joint Registration*: Before a point cloud registration algorithm can be applied to the point clouds, they must be pre-processed. First, the point clouds are transformed into the global frames  $\{R_1^i\}$  and  $\{R_2^j\}$  with the vehicle pose estimates belonging to the respective measurement timestamps. Then, we separate the target points from the ground points by using the Random Sample Consensus (RANSAC) [28] algorithm

to identify and filter out the ground plane. Finally, we use GMMCalib [10] for joint registration of the filtered point clouds into a common calibration frame  $\{C\}$ . GMMCalib returns the registration transform  $C_{R_1} T$  and  $C_{R_2} T$  for each point cloud needed for the optimization procedure. Furthermore, it provides the reconstructed target shape in the calibration frame in the form of a point cloud.

3) *Minimization Algorithm*: To implement a minimization algorithm, it is necessary to define a cost function to be minimized. As shown in Eq. 3, the cost function is formulated as the sum of all pairwise errors between the estimated calibration frame errors. Note that the previously discussed problem statement assumes that the vehicle poses and calibration transformations are accurate. Therefore, errors introduced by the registration algorithm or the kinematic model may negatively affect the calibration result. To account for such erroneous approximations, we introduce an outlier filter that removes the most extreme outliers of the computed errors. For this purpose, we introduce the parameter  $k$ . After computing all pairwise errors between calibration frame estimates, we disregard all errors that are below the  $k^{\text{th}}$  percentile or above the  $(100 - k)^{\text{th}}$  percentile. We set  $k$  to 10 in our implementation, as this proved to produce the best results for both ground truth and UKF poses.

The application of an outlier filter introduces a non-differentiable cost function, as increasing or decreasing an error value may cause discontinuous transitions in and out of the defined percentiles. Therefore, a minimization algorithm that can handle such functions is needed. Consequently, Powell's conjugate direction method [29] is implemented to solve the minimization problem.

The error function  $e$  introduced in Eq. 3 computes the error between two estimates  $C_{R_a} \bar{T}_a^i$  and  $C_{R_b} \bar{T}_b^j$  of the calibration frame error transformation. In our implementation, we distinguish between the rotational and translational parts of the inverse of both transformations. Inverting the transformations allows to apply them to a set of points in the calibration frame  $\{C\}$ . To calculate the error between two transformations, their rotational parts are applied to such a set of points. The errors of the rotational parts are the squared pairwise distances between corresponding transformed points. The additional translation error is simply the squared pairwise difference. As GMMCalib returns the reconstructed shape of the target object, we define the points of the oriented bounding box of this shape to be the point set for this error function.

## IV. EXPERIMENT DESIGN

In this chapter, we present the experimental setup used to evaluate our proposed framework. The simulation is performed in the driving simulator CARLA [30] and consists of the digital twin of the research vehicle EDGAR [31], a generic calibration target, and a flat surface. To validate our approach, the experiments are also performed in a real-world environment with the research vehicle EDGAR. Furthermore, we describe the evaluation metrics of the S2S and S2V calibration performance.

### A. Simulation Setup

In both the simulation and the real world, the vehicle is equipped with two LiDARs with a non-overlapping FoV. One LiDAR is mounted on the front end of the vehicle roof at the position  $[2 \ 0 \ 2]^T$  and is rotated  $-10^\circ$  around the y-axis. It, therefore, faces the driving direction and is tilted to the ground. The other LiDAR is mounted to the roof's rear end at the position  $[-0.4 \ 0 \ 2]^T$  and is also rotated  $-10^\circ$  around the y-axis and additionally  $180^\circ$  around the z-axis. This means that the rear LiDAR is facing the opposite direction of travel and is also tilted towards the ground. These exact mounting positions are given for the simulation, but correspond to the expected positions of the real vehicle. The characteristics of the simulated sensors, listed in Table I, are chosen to match those of real-world sensors. The resulting LiDAR FoVs are qualitatively shown in the optimization part of Fig. 1.

Sensor	Attribute	Dimension	Value
LiDAR	Horizontal FoV [ $^\circ$ ]	-	120
LiDAR	Vertical FoV [ $^\circ$ ]	-	25
LiDAR	Range [m]	-	500
LiDAR	Channels [-]	-	152
LiDAR	Noise [m]	(x,y,z)	0.01
Accelerometer	Noise [ $\frac{m}{s^2}$ ] (x,y,z)	0.05	
Gyroscope	Noise [ $\frac{rad}{s}$ ]	(x,y,z)	0.005
GPS	Noise [ $^\circ$ ]	(lat,lon)	1.5e-7
GPS	Noise [m]	(alt)	0.02
Orientation	Noise [rad]	(x,y,z)	0.005
Velocity	Noise [ $\frac{m}{s}$ ]	(x,y,z)	0.1

TABLE I: Sensor Characteristics of the CARLA simulation

The simulated vehicle is also equipped with an IMU (accelerometer and gyroscope) and GPS. All sensors and additional data are augmented by an artificially added Gaussian noise. As a calibration target we use a plastic chair. It should be noted, however, that any target can be used for these experiments. The only requirements are that the target should be detectable by the LiDAR sensor and for non-overlapping FoVs it is a prerequisite to use non-symmetric targets with respect to the observed perspectives. In the real-world experiments, an additional cubic target is placed at a position that is not part of the optimization as described in Section III to serve as a validation target (see Fig. 6). Another important consideration is the robot maneuver, since certain S2V errors are not observable for some trajectories. We use the work of [5] as a basis for these considerations, which primarily uses curves for S2V calibration. The trajectory used in the simulation is shown in Fig. 1 and was executed with an average velocity of  $2\frac{m}{s}$  and a static steering angle of about  $17^\circ$ . These values are chosen such that they fulfill maximum observability for the S2V calibration and require minimal space for the robot maneuver. The real-world setup is shown in Fig. 6 and is analogous to the simulated environment.

### B. Evaluation

In the simulation, the ground truth LiDAR transformations relative to the vehicle frame are known. These are denoted

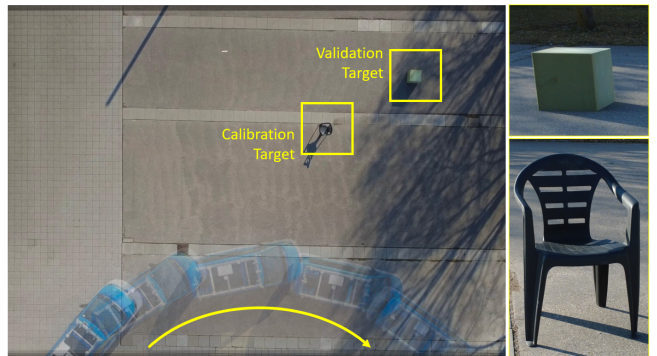


Fig. 3: **Left:** Curved maneuver with the EDGAR [31] in the real-world setup. **Right:** A chair as a calibration target and the cubic validation target.

as  ${}^V_{L_1}T$  and  ${}^V_{L_2}T$  for LiDAR  $L_1$  and  $L_2$ , respectively. After the optimization, estimates for corrected LiDAR transformations are computed. However, these corrections might still contain errors. Therefore, we define the LiDAR transformation estimates as  ${}^{V_1}_{L_1}T$  and  ${}^{V_2}_{L_2}T$  for  $L_1$  and  $L_2$ , respectively. Using these four transformations, the S2S and S2V calibration errors can now be computed separately. The  $L_1$  S2V errors can be computed directly by computing the residual of  ${}^{V_1}_{L_1}T$  relative to  ${}^V_{L_1}T$ . Equivalently, the  $L_2$  S2V errors are equal to the residual of  ${}^{V_2}_{L_2}T$  relative to  ${}^V_{L_2}T$ . To compute the residual of one transformation matrix relative to another in this context, the homogeneous transformations are first converted into translation vectors and Euler angles. Then, the pairwise residuals are computed to distinguish between different translation and rotation errors. Thus, the residual of an estimated transformation is the vector of its translation and rotation residuals and is evaluated accordingly.

The evaluation of the S2S calibration results is less straightforward, since there are remaining S2V errors in  ${}^{V_1}_{L_1}T$  and  ${}^{V_2}_{L_2}T$ . Let us define  $L_2$  as the reference sensor and, therefore, define its S2V transformation as fixed. We now need to calculate  ${}^{V_1}_{L_1}T^*$  so that  ${}^{V_1}_{L_1}T^*$  contains no S2S calibration error relative to  ${}^{V_2}_{L_2}T$ .  ${}^{V_1}_{L_1}T^*$  can be constructed as follows:

$${}^{V_1}_{L_1}T^* = {}^{V_2}_{L_2}T {}^{V_1}_{L_2}T^{-1} {}^{V_1}_{L_1}T \quad (6)$$

In other words,  ${}^{V_1}_{L_1}T^*$  describes the ground truth pose of  $L_1$  relative to the erroneous vehicle frame, containing the S2V error of  $L_2$ . The S2S calibration error can now be defined as the residual of  ${}^{V_1}_{L_1}T$  relative to  ${}^{V_1}_{L_1}T^*$ .

In our experiments, we added randomly generated errors to the ground truth transformations of  $L_1$  and  $L_2$  to get erroneous estimates. The translation errors for x, y and z are uniformly distributed in the range of  $-0.1m$  to  $0.1m$ . The rotation errors for roll, pitch and yaw are also uniformly distributed, but in the range of  $-3.0^\circ$  to  $3.0^\circ$ . In total, we run 100 simulations containing ground truth poses and erroneous UKF poses.



## V. RESULTS & DISCUSSION

### A. S2S Calibration

In this section, we evaluate our method regarding S2S calibration and compare the results for ground truth and UKF poses. In addition, we will compare our method with mlcc [23]. Due to the fact that no comparable target-based approach currently exists, we compare this targetless framework because it supports non-overlapping FoVs. For the sake of comparison, we will perform the motion proposed in Section IV-A for both algorithms. The work of [23] is evaluated with ground truth vehicle poses. The mean calibration errors of all executions are shown in Table II.

Algorithm	$\delta x$	$\delta y$	$\delta z$	$\delta \phi$	$\delta \theta$	$\delta \psi$
mlcc [23]	5.5642	0.4691	2.2511	0.1116	0.3222	0.1286
CaLiV (UKF)	<b>0.0011</b>	0.0154	0.0200	0.0043	0.0070	<b>0.0005</b>
CaLiV (GT)	0.0124	<b>0.0038</b>	<b>0.0088</b>	<b>0.0007</b>	<b>0.0006</b>	0.0015

TABLE II: Mean S2S translation and rotation errors in  $m$  and  $rad$ , respectively, using UKF and ground truth (GT) poses. mlcc comparison is performed using GT poses.

The adaptive voxelization-based work of [23] produces rather inaccurate calibration transformations in our experiments. The mean translation errors are up to several meters, while the mean rotation errors are in the range of  $6^\circ$  to  $19^\circ$ . The main reason is that when exposed to erroneous LiDAR poses that are due to calibration errors, mlcc does not provide accurate results. In their work, Liu *et al.* state that the initial LiDAR extrinsic parameters should be pre-calibrated and accurate LiDAR poses must be available, e.g. by first applying a hand-eye calibration or SLAM. From our results, we conclude that the initial S2V errors of up to  $3^\circ$  introduced in our experiment cannot be handled by mlcc and a more accurate prior calibration is necessary.

When evaluating the results of the proposed framework, we observe that the mean calibration errors of the execution with ground truth poses is not necessarily better than the execution with UKF poses in all dimensions. The mean x-error is  $0.11cm$  for UKF poses, which is more accurate than the  $1.24cm$  for ground truth poses. In addition, the mean yaw ( $\psi$ ) error is around  $0.03^\circ$  for UKF poses and  $0.09^\circ$  for ground truth poses. However, all other calibration errors are still significantly more accurate when using ground truth poses. This behavior shows that the resulting calibration accuracy highly depends on the accuracy of the vehicle poses, however, the more accurate calibration results for the UKF poses indicate that also the registration and optimization algorithm has a high influence even in the presence of ground truth poses.

Fig. 4 shows the calibration errors' distributions of our proposed algorithm for UKF and ground truth poses. Although there are outliers, they are relatively close to the median. Furthermore, the standard deviations are relatively low for all errors. The calibration with ground truth poses is especially reliable. The biggest difference between the results of UKF and ground truth poses is in the pitch ( $\theta$ )

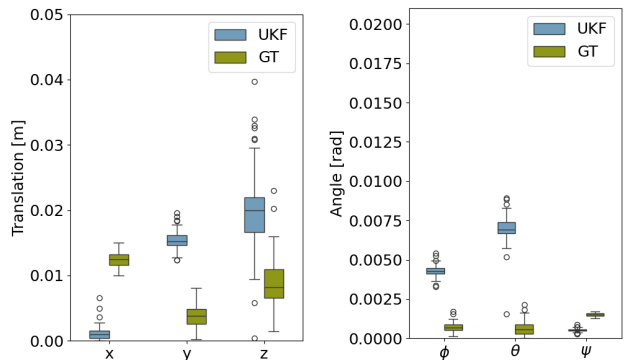


Fig. 4: The distribution of the S2S translation and rotation errors of CaLiV using UKF (blue) and ground truth (green) poses.

errors. Nevertheless, the maximum error of all calibrations with UKF poses is below  $0.6^\circ$  and the median is around  $0.43^\circ$ .

An important question when calculating the S2S calibration is why it is even needed, since the S2V calibration is performed for both sensors. Experimental results show that performing S2S calibration as a first step improves the overall accuracy of the subsequent S2V calibration. This pre-alignment improves the consistency between sensor measurements, resulting in more accurate S2V calibration results. To demonstrate the robustness of our approach against the extremest perspective differences, we chose a sensor setup that represents the worst-case scenario in terms of non-overlapping sensor coverage.

### B. S2V Calibration

In the following, we present the S2V calibration results and compare them for ground truth and UKF poses. In addition, we distinguish between the  $L_1$  and  $L_2$  S2V calibration error. Since  $L_2$  is the reference LiDAR, the  $L_1$  S2V error is dependent on the  $L_2$  S2V error and the S2S error. As described in Section III, the second stage of the calibration process makes use of the previously calibrated S2S transformations. For the S2V calibration, an additional constraint must be introduced: The remaining transformation to be optimized by the minimization algorithm is the S2V error  $\sqrt{V^2} \bar{T}$ . In order to compute the rotation errors independently from the translation errors, the S2V translation errors are fixed to zero. This means, the minimization only optimizes the S2V rotation errors. Table III shows the mean  $L_1$  and  $L_2$  S2V roll ( $\phi$ ), pitch ( $\theta$ ) and yaw ( $\psi$ ) errors after performing 100 calibrations. Again, the calibration accuracy is evaluated for both the UKF and ground truth poses. Since only the rotation errors are aimed to be solved here, we do not evaluate the translation errors. The roll and pitch errors are both less than  $0.1^\circ$ . The mean S2V yaw errors of  $L_1$  and  $L_2$  for both UKF and ground truth poses are all below  $0.5^\circ$ . Fig. 5 shows the distributions of 100  $L_1$  (left figure) and  $L_2$  (right figure) S2V rotation errors in radian for both UKF and ground truth poses after the S2V calibration. The roll and pitch distributions have a low standard deviation and few

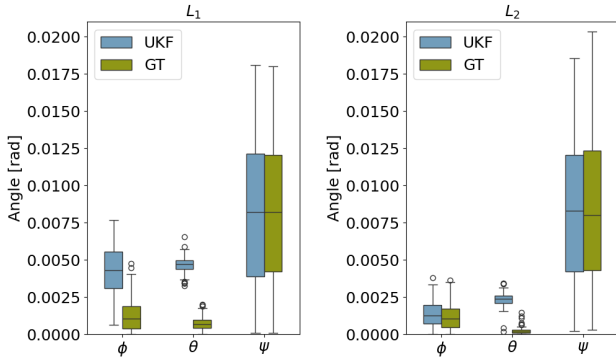


Fig. 5: The distribution of the S2V rotation errors of CaLiV using UKF (blue) and ground truth (green) poses. The distributions for  $L_1$  are shown on the left, while the right plot shows the distributions of the  $L_2$  errors.

outliers. All roll and pitch errors are below  $0.5^\circ$ . Although the standard deviation of the yaw errors and the number of outliers are noticeably bigger, the mean is close to the median and the maximum errors are a little over  $1^\circ$ .

LiDAR	Poses	$\delta\phi$	$\delta\theta$	$\delta\psi$
$L_1$	UKF	0.0042	0.0047	<b>0.0082</b>
	GT	<b>0.0013</b>	<b>0.0007</b>	0.0084
$L_2$	UKF	0.0014	0.0024	<b>0.0083</b>
	GT	<b>0.0012</b>	<b>0.0002</b>	0.0084

TABLE III: Mean S2V rotation errors in *rad* of this work’s algorithm for the curved trajectory. The proposed method is evaluated for both ground truth and UKF poses.

Algorithm	$\delta\phi$	$\delta\theta$	$\delta\psi$
Multi-LiCa [16]	-	0.0056	-
SensorX2Car [18]	0.0046	0.0019	-
CaLiV (Ours)	<b>0.0013</b>	<b>0.0007</b>	<b>0.0084</b>

TABLE IV: Mean rotation errors in *rad* for the curved trajectory. To compare the calibration performance only the calibration was performed using GT poses.

The S2V calibration performance of CaLiV is compared to the two open-source calibration methods Multi-LiCa [16] and SensorX2Car [18]. Both methods compute the partial LiDAR-to-Vehicle calibration using the ground plane to estimate the pitch and roll angles. The results are shown in Table IV. Note that Multi-LiCa and SensorX2Car do not provide the calibration transformation for all rotation angles, and therefore, only the roll estimates for Multi-LiCa and the roll and pitch angles for the SensorX2Car calibration algorithm can be compared. For the comparison with CaLiV, we use the ground truth poses to evaluate the calibration accuracy only. We outperform both S2V approaches using ground truth poses and, compared to SensorX2Car, we are slightly less accurate using UKF poses only in the pitch angle error.

We want to highlight the accuracy of the calibration with respect to the rotational components and also discuss the translation components. In the experiments, we observe that

the translational  $z$ -component is not observable with our trajectory. In addition, our algorithm could not distinguish between translational  $x$ -error and yaw error. The rotational errors are considered to be the most important for autonomous driving tasks, since they increase with distance and therefore pose a safety concern [10]. More specifically, from a purely geometric point of view, a S2V yaw error of  $1^\circ$  corresponds to a lateral displacement of an object of nearly  $2m$  at a distance of  $100m$ . Since translation errors remain constant over distance, we assume that there are no translation errors and focus on the rotation errors in the S2V optimization. At the cost of possible S2V translation errors, this assumption leads to more accurate S2V calibration results overall.

It is important to note that CaLiV cannot be used in real time, but rather as an offline algorithm. The current computation time of the algorithm is about 20 minutes, mainly due to the optimization step.

### C. Real World

We validate CaLiV in real-world experiments as described in Section IV. Since no ground truth of the transformation between the front and rear LiDAR is available in real-world environments, the real-world performance is evaluated qualitatively on the validation target. It should be noted

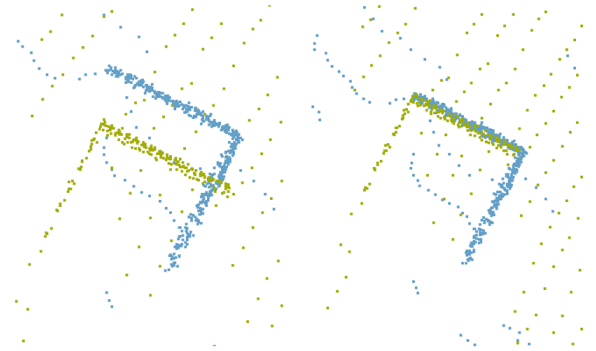


Fig. 6: **Left:** Point cloud of the validation target before the calibration (green: rear LiDAR, blue: front LiDAR). **Right:** Point clouds of the validation target after the calibration.

that no prior sensor calibration was performed, resulting in relatively high initial calibration errors as shown on the left of Fig. 6. The figure shows the first frame of the front LiDAR at the beginning of the trajectory and the last frame of the rear LiDAR at the end of the trajectory. This gives a better insight into the overall ability of CaLiV to compensate for the propagating S2V calibration error over time/distance. After performing the calibration with CaLiV, the validation target seen on the right side of Fig. 6 is well aligned, indicating a successful S2V calibration.

To achieve these results, a number of criteria must be met in the real experiments. To account for the motion distortion of the LiDAR sensors and the distortion of the angular velocities during the curved trajectory, the vehicle motion must be stationary and at a constant velocity of about  $5 \frac{m}{s}$ . Furthermore, real-world LiDAR sensors do not have homogeneous point resolution across the vertical and horizontal

FoV, resulting in sparse point clouds at the edges of the FoV. In our experiments, this required an additional voxel and outlier filter to account for the differences in cardinality and improve the registration results during calibration.

## VI. CONCLUSION & FUTURE WORK

The goal of this work was to provide a target-based framework for S2S and S2V calibration of multi-LiDAR systems with arbitrary FoV overlap. In addition, we aimed to develop an algorithm that is independent of environmental features, does not rely on external sensors, and supports arbitrary target shapes that can be registered from different perspectives. The main focus is to present the challenges of target-based S2S and S2V calibration and the methodology developed to address these challenges. CaLiV demonstrates high accuracy and robustness for both S2S and S2V calibration, and is the first target-based framework to solve both tasks simultaneously without the need for external sensing devices. We present a benchmark for both calibration tasks independently and compare our work with openly available calibration methods. CaLiV outperforms the current state of the art in both non-overlapping sensor calibration and S2V calibration. Another advantage of CaLiV is that it is particularly suitable for end-of-line calibration where space is limited. While our current method requires a curved trajectory to optimize S2S and S2V calibration, it remains to be investigated whether moving the target would yield equally accurate results. Furthermore, the possibility of using a more complex trajectory could be explored to also solve the S2V translation errors while maintaining the accuracy.

## REFERENCES

- [1] D. J. Yeong, G. Velasco-Hernandez, J. Barry, and J. Walsh, "Sensor and sensor fusion technology in autonomous vehicles: A review," *Sensors*, vol. 21, pp. 1–37, 3 2021.
- [2] R. Horaud and F. Dornaika, "Hand-eye calibration," *The International Journal of Robotics Research*, vol. 14, pp. 195–210, 1995.
- [3] S. Das, N. Mahabadi, A. Djikic, C. Nassir, S. Chatterjee, and M. Fallon, "Extrinsic calibration and verification of multiple non-overlapping field of view lidar sensors," in *2022 International Conference on Robotics and Automation (ICRA)*, 5 2022.
- [4] R. Kümmerle, G. Grisetti, C. Stachniss, and W. Burgard, "Simultaneous parameter calibration, localization, and mapping for robust service robotics," in *Advanced Robotics and its Social Impacts*, pp. 76–79.
- [5] S. Das, L. A. Klinteberg, M. Fallon, and S. Chatterjee, "Observability-aware online multi-lidar extrinsic calibration," *IEEE Robotics and Automation Letters*, vol. 8, pp. 2860–2867, 5 2023.
- [6] P. An, J. Ding, S. Quan, J. Yang, Y. Yang, Q. Liu, and J. Ma, "Survey of extrinsic calibration on lidar-camera system for intelligent vehicle: Challenges, approaches, and trends," *IEEE Transactions on Intelligent Transportation Systems*, pp. 1–25, 7 2024.
- [7] J. Dombhof, J. F. Kooij, and D. M. Gavrilu, "A joint extrinsic calibration tool for radar, camera and lidar," *IEEE Transactions on Intelligent Vehicles*, 2021.
- [8] N. Charron, S. L. Waslander, and S. Narasimhan, "A target-based extrinsic calibration framework for non-overlapping camera-lidar systems using a motion capture system," 3 2023.
- [9] L. Wiesmann, T. Läbe, L. Nunes, J. Behley, and C. Stachniss, "Joint intrinsic and extrinsic calibration of perception systems utilizing a calibration environment," *IEEE Robotics and Automation Letters*, 2024.
- [10] I. Tahiraj *et al.*, "GMMCalib: Extrinsic Calibration of LiDAR Sensors using GMM-based Joint Registration," in *IEEE International Conference on Intelligent Robots and Systems(IROS)*, 2024.
- [11] P. Wei, G. Yan, Y. Li, K. Fang, X. Cai, J. Yang, and W. Liu, "Croon: Automatic multi-lidar calibration and refinement method in road scene," in *IEEE International Conference on Intelligent Robots and Systems*, vol. 2022-October, 2022, pp. 12 857–12 863.
- [12] M. A. de Miguel, C. Guindel, A. Al-Kaff, and F. Garcia, "High-accuracy patternless calibration of multiple 3-d lidars for autonomous vehicles," *Lenguas Modernas*, vol. 23, pp. –209, 6 2023.
- [13] S. Nijjima, A. Suzuki, R. Tsuzaki, and M. Kinoshita, "Extrinsic calibration of multiple lidars for a mobile robot based on floor plane and object segmentation," 3 2024.
- [14] J. Xu, S. Huang, S. Qiu, L. Zhao, W. Yu, M. Fang, M. Wang, and R. Li, "Lidar-link: Observability-aware probabilistic plane-based extrinsic calibration for non-overlapping solid-state lidars," *IEEE Robotics and Automation Letters*, vol. 9, pp. 2590–2597, 3 2024.
- [15] S. W. Meyer, H. Chen, and D. M. Bevy, "Automatic extrinsic rotational calibration of lidar sensors and vehicle orientation estimation," in *IFAC-PapersOnLine*, vol. 54. Elsevier B.V., 11 2021, pp. 424–429.
- [16] D. Kulmer, I. Tahiraj, A. Chumak, and M. Lienkamp, "Multi-lica: A motion- and targetless multi - lidar-to-lidar calibration framework," in *IEEE International Conference on Multisensor Fusion and Integration for Intelligent Systems*, 2024.
- [17] N. Heide, T. Emter, and J. Peterleit, "Calibration of multiple 3d lidar sensors to a common vehicle frame," in *ISR 2018; 50th International Symposium on Robotics*, 2018.
- [18] G. Yan, Z. Luo, Z. Liu, Y. Li, B. Shi, and K. Zhang, "Sensorx2vehicle: Online sensors-to-vehicle rotation calibration methods in road scenarios," *IEEE Robotics and Automation Letters*, vol. 9, pp. 3775–3782, 4 2024.
- [19] X. Liu and F. Z. Zhang, "Extrinsic calibration of multiple lidars of small fov in targetless environments," *IEEE Robotics and Automation Letters*, vol. 6, pp. 2036–2043, 4 2021.
- [20] D. Chang, R. Zhang, S. Huang, M. Hu, R. Ding, and X. Qin, "Versatile multi-lidar accurate self-calibration system based on pose graph optimization," *IEEE Robotics and Automation Letters*, vol. 8, pp. 4839–4846, 8 2023.
- [21] J. Jiao, Y. Yu, Q. Liao, H. Ye, and F. Rui, "Automatic calibration of multiple 3d lidars in urban environments," in *IEEE International Conference on Intelligent Robots and Systems (IROS)*, 2019.
- [22] J. Lin, X. Liu, and F. Zhang, "A decentralized framework for simultaneous calibration, localization and mapping with multiple lidars," in *2020 IEEE/RSJ International Conference on Intelligent Robots and Systems (IROS)*, 7 2020, pp. 4870–4877.
- [23] X. Liu, C. Yuan, and F. Zhang, "Targetless extrinsic calibration of multiple small fov lidars and cameras using adaptive voxelization," *IEEE Transactions on Instrumentation and Measurement*, vol. 71, 2022.
- [24] J. Zhang, Q. Lyu, G. Peng, Z. Wu, Q. Yan, and D. Wang, "Lb-l2-calib: Accurate and robust extrinsic calibration for multiple 3d lidars with long baseline and large viewpoint difference," in *Proceedings - IEEE International Conference on Robotics and Automation*, 2022, pp. 926–932.
- [25] Z. Li, H. Dong, D. Liu, and Y. Ding, "Extrinsic calibration of a 2d laser rangefinder and a depth-camera using an orthogonal trihedron," in *IEEE International Conference on Intelligent Robots and Systems*, vol. 2022-October, 2022, pp. 6264–6269.
- [26] J. J. Craig, *Introduction to Robotics Mechanics and Control Third Edition*. Pearson Education, 2005.
- [27] S. J. Julier and J. K. Uhlmann, "New extension of the kalman filter to nonlinear systems," in *Defense, Security, and Sensing*, 1997.
- [28] M. A. Fischler and R. C. Bolles, "Random sample consensus: a paradigm for model fitting with applications to image analysis and automated cartography," *Commun. ACM*, vol. 24, pp. 381–395, 1981.
- [29] M. J. D. Powell, "An efficient method for finding the minimum of a function of several variables without calculating derivatives," *The Computer Journal*, vol. 7, no. 2, pp. 155–162, 01 1964.
- [30] A. Dosovitskiy, G. Ros, F. Codevilla, A. Lopen, and V. Koltun, "Carla: An open urban driving simulator," 1 2017.
- [31] P. Karle *et al.*, "Edgar: An autonomous driving research platform – from feature development to real-world application," 1 2024.